Smoothed Particle Hydrodynamics Modeling of Thermal Barrier Coating Removal Process Using Abrasive Water Jet Technique

Jian Zhang[1], Xuehui Yang[1], Sugrim Sagar[1], Tejesh Dube[1], Dan Daehyun Koo[2], Bong-Gu Kim[3], Yeon-Gil Jung[3], Jing Zhang[1*]

1. Department of Mechanical and Energy Engineering, Indiana University - Purdue University Indianapolis, Indianapolis, Indiana, USA

2. Department of Engineering Technology, Indiana University - Purdue University Indianapolis, Indianapolis, Indiana, USA

3. Department of Materials Convergence and System Engineering, Changwon National University, Changwon, Republic of Korea

Corresponding author: jz29@iupui.edu

Abstract

In this work, a new smoothed particle hydrodynamics (SPH) based model is developed to simulate the removal process of thermal barrier coatings (TBCs) using the abrasive water jet (AWJ) technique. The effects of water jet abrasive particle concentration, incident angle, and impacting time on the fracture behavior of the TBCs are investigated. The Johnson-Holmquist plasticity damage model (JH-2 model) is used for the TBC material, and abrasive particles are included in the water jet model. The results show that the simulated impact hole profiles are in good agreement with the experimental observation in the literature. Both the width and depth of the impact pit holes increase with impacting time. The deepest points in the pit hole shift gradually to the right when a

This is the author's manuscript of the article published in final edited form as:

Zhang, J., Yang, X., Sagar, S., Dube, T., Koo, D. D., Kim, B.-G., Jung, Y.-G., & Zhang, J. (2022). Smoothed Particle Hydrodynamics Modeling of Thermal Barrier Coating Removal Process Using Abrasive Water Jet Technique. Journal of Manufacturing Science and Engineering, 144(091012). https://doi.org/10.1115/1.4055048

30° water jet incident angle is used because the water jet comes from the right side, which is more effective in removing the coatings on the right side. A higher concentration of abrasive particles increases both the width and depth, which is consistent with the experimental data. The depths of the impact pit holes increase with the water jet incident angle, while the width of the impact holes decreases with the increase of the water jet incident angle. The water jet incident angle dependence can be attributed to the vertical velocity components. The erosion rate increases with the incidence angle, which shows a good agreement with the analytical model. As the water jet incident angle increases, more vertical velocity component contributes to the kinetic energy which is responsible for the erosion process.

Keywords: Smoothed particle hydrodynamics; thermal barrier coating; erosion, removal process; abrasive water jet

1 Introduction

Ceramic coatings are used in the high-temperature sections of gas turbine engines for improved efficiency due to their low thermal conductivity and mechanical properties[1]. A typical TBC topcoat is made of yttria-stabilized zirconia (YSZ) and a bond coat of MCrAlY. TBCs should resist chemical, mechanical, and thermal stresses resulting from the gas turbine operating conditions. However, due to coating degradation or foreign object damage, a routine maintenance and repair process is needed, including the removal of the damaged coatings [2, 3]. A recent review of ceramic coating removal and repair techniques is given in Ref. [3].

Among different techniques, abrasive waterjet (AWJ) has become a promising machining process to remove damaged coatings. AWJ is formed by mixing high-pressure waterjets with abrasive particles. The process has several advantages, such as relatively low cost compared to the laser-based process. It provides a clean and green solution that can be more cost-effective than traditional acid stripping and grit blasting for removing coatings from turbine components. It also enables the penetration of thick cross-sections and has minimum stresses and small cutting forces on the parts [4-6]. Understanding the effects of the controlling factors (e.g., abrasive concentration, impact angle, impact time, and standoff distance) on the AWJ performance is essential to enhancing the machining performance of the process [7]. In Ref. [8], the effects of processing parameters, such as incident angle, impacting time, and abrasive particle concentration were investigated using a single-factor experiment. It is concluded that the AWJ process is an effective way to remove TBCs [8]. The effects of abrasive particle concentration on the impact performance of the AWJ were studied in Ref. [9], and the study showed that the mean impact force tends to increase linearly with the abrasive concentration [9]. In Ref. [6], as shown in the precision AWJ process is reported.

Combined with a 5-axis computer numerically controlled (CNC), the AWJ removes the coating in iterative steps.

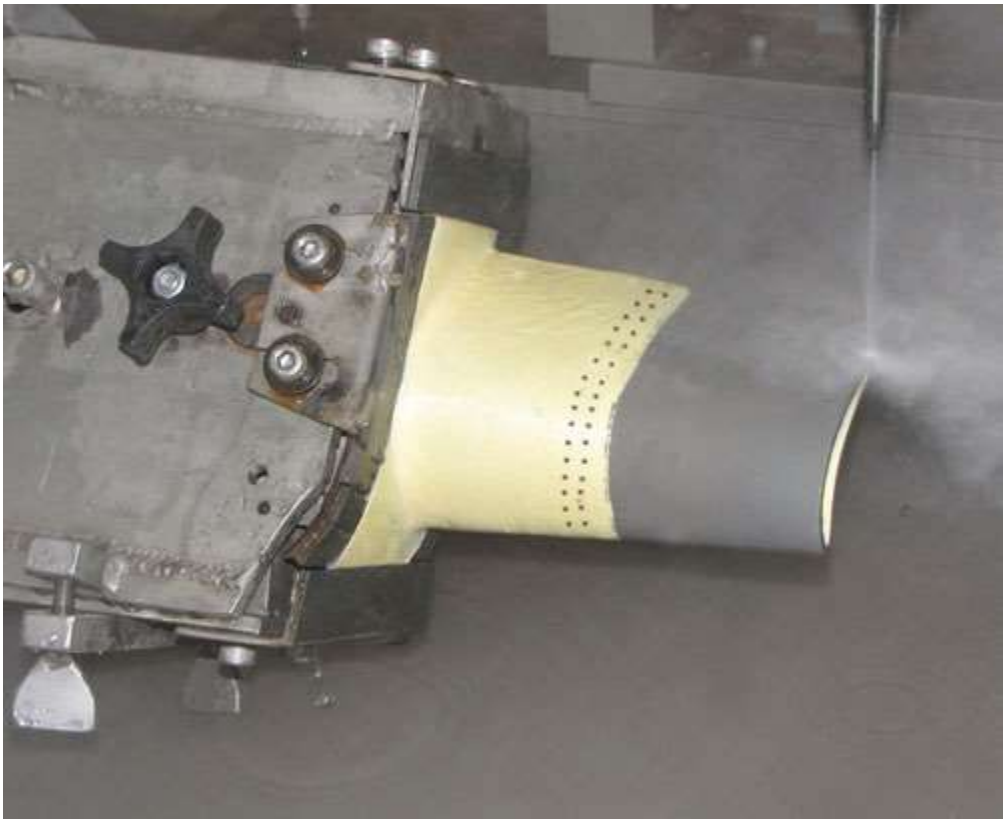

Figure 1: A precision abrasive waterjet process removing thermal barrier coating from a turbine blade component [6].

There are a few modeling studies on the optimization of the AWJ process. The Smoothed Particle Hydrodynamics (SPH) and Arbitrary Lagrangian-Eulerian (ALE) methods were employed to study the depth of water jet penetration and erosion mechanism in Ref. [10]. The SPH coupled finite element method (FEM) was adopted to simulate the abrasive water jet cutting progress in Ref. [11]. In addition, a statistical model was established to understand the effect of abrasive waterjet cutting parameters on the surface roughness [5]. The results show that improved surface roughness can be achieved by increasing the water pressure at low traverse speeds, or decreasing

the pressure at high traverse speeds, or decreasing the standoff distance at low traverse speeds and low pressures in the investigating range [5]. In Ref. [12], an analytical model was developed to determine the heat flux at the contact surface during the AWJ machining process. The generated heat due to plastic deformation is diminished because the high-velocity waterjet serves as a coolant removing the heat through convection [12].

Despite the previous studies presented above, a systematic understanding of the fundamental mechanism of the AWJ process to remove TBCs is still missing, which hinders the full potential of the process. In this work, an SPH-based model to simulate the TBC removal process using the AWJ technique is proposed. The effects of abrasive particle concentration, incident angle, and impacting time on the TBC fracture are studied. The simulation results are compared against the experimental data and analytical model in the literature. It is helpful to deeply understand the fundamental mechanism of the AWJ process to remove TBCs.

2 Model description

2.1 SPH method

A brief introduction of the governing equations in the SPH method is presented below. For comprehensive reviews, readers may refer to, e.g., Refs. [13, 14]. The SPH method is a mesh-free or meshless method. An approximate solution is obtained based on the nodal data that are distributed within the computational domain. In this numerical method, a function f is approximated by multiplying f with a smoothing kernel function, and then integrating over the computational domain as follows [15].

$$< f(x) >= \int_{\Omega} f(x')W(x - x', h)dx' \quad (1)$$

where x and x' denote the position vectors at different points and W is the kernel function.

Equation 1 can be discretized into a form of summation over all the nearest neighboring particles inside the region controlled by the smoothing length for a given particle j at a certain instant of time:

$$f(r) \approx \sum_{j=1}^{N} \frac{m_j}{\rho_j} f(r_j)\ \mathrm{W}\ (\mathrm{r}\text{-}r_j, h) \quad (2)$$

where m and ρ are the mass and density of a particle, respectively, and h is a smoothing length to control the size of the summation domain.

2.2 SPH model details

2.2.1 Geometry of the model

The SPH model of the TBC removal process is shown in Figure 2. The model includes abrasive particles, a water jet, and a TBC layer. The composition of the TBC layer is assumed to be zirconia (ZrO_2) since the SPH model parameters for yttria-stabilized zirconia are sparse. The abrasive particles are alumina (Al_2O_3) particles. The nozzle diameter is set to 200 μm, which is the same as the experiment in Ref. [16]. The TBC layer's dimensions are 2000×2000×500 μm^3. All the surfaces of the TBC layer are fixed except the top one. The water jet incident angle is defined as the angle between the water jet and the top surface of the TBC layer, as shown in Figure 2. The abrasive concentration is the number ratio between the abrasive particle to the sum of abrasive particles and water particles.

A random function was used to replace the water particle with the abrasive particles' positions and sizes based on their concentrations. This was done by coding in MATLAB.

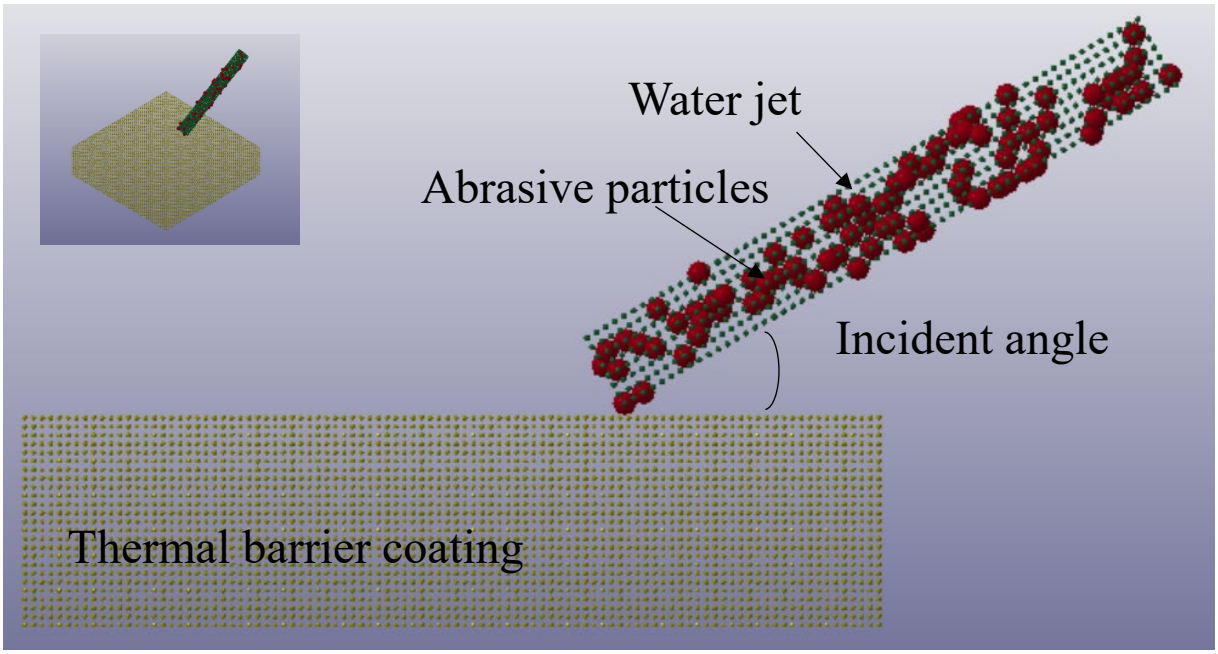

Figure 2: The side view of the SPH model for the TBC layer removal using the AWJ process. The abrasive particles in the water jet are enlarged to show their existence. The inset shows the 3D view of the SPH model.

2.2.2 Material constitutive model

For the ZrO_2 TBC layer, the Johnson-Holmquist plasticity damage model (JH-2 model) is used, which has been proven suitable for ceramics, glass, and other brittle materials [17]. In the JH-2 model, the equivalent stress for a ceramic-type material is given by[18]:

$$\sigma^* = \sigma_i^* - D\,(\sigma_i^* - \sigma_f^*) \tag{3}$$

where D is the damage parameter. The superscript asterisk (*) indicates a normalized quantity. σ_i^* is determined by:

$$\sigma_i^* = a\,(p^* + t^*)\,n\,(1 + c\ln \dot{\varepsilon}^*) \tag{4}$$

which represents the intact and undamaged behavior. a is the intact normalized strength parameter, c is the strength parameter for strain rate dependence, and $\dot{\varepsilon}^*$ is the normalized plastic strain rate.

Also

$$t^* = \frac{T}{PHEL} \tag{5}$$

$$p^* = \frac{\mathrm{p}}{\mathrm{PHEL}} \tag{6}$$

where T is the maximum tensile pressure strength, $PHEL$ is the pressure component at the Hugoniot elastic limit and P is the pressure.

In an undamaged material in compression, the hydrostatic pressure is given by:

$$P = k_1\mu + k_2\mu^2 + k_3\mu^3 \tag{7}$$

And in tension, it becomes:

$$P = k_1\mu \tag{8}$$

where the compression factor $\mu = \rho/\rho_0 - 1$, and ρ/ρ_0 is the ratio of current density to initial density [19].

Additionally, the damage parameter D is determined by:

$$D = \sum \frac{\Delta\varepsilon^{\mathrm{p}}}{\varepsilon_f^{\mathrm{p}}} \tag{9}$$

which represents the accumulated damage based upon the increase in plastic strain per computational cycle. The plastic strain to fracture is:

$$\varepsilon_f^p = d_1(p^* + t^*)^{d2} \tag{10}$$

where the parameter d_1 controls the rate at which damage accumulates:

$$\sigma_f^* = b(p*)^m (1 + c \ln\dot{\varepsilon}*) \tag{11}$$

For the water jet and abrasive particles, the pressure is calculated by the state equation Mie-Grueisen as follows:

$$p = \frac{\rho_0 C^2 \mu[1+(1-\gamma/2)\mu-(\alpha/2)\mu^2]}{[1-(S_1-1)\mu-S_2\mu^2/(\mu+1)-S_3\mu^3/(1+\mu)]^2} + (\gamma + \alpha\mu)E_0 \tag{12}$$

where p is pressure; S_1, S_2, and S_3 are the coefficients of the slope of the $U_s - U_p$ curve, where U_s and U_p are the shock velocity and particle velocity, respectively; γ is the Grüneisen factor; C is the intercept of the $U_s - U_p$ curve; E_0 is the internal energy; α is the volume correction factor.

2.2.3 Material properties

The ZrO_2 in the TBC layer has the following properties: density is 5850 kg/m^3, the shear modulus is 95.31GPa, tensile strength is 0.2 GPa, and the Poisson's ratio is 0.22. The coefficient values in the JH-2 model used for the TBC are listed in Table 1[20].

Table 1: JH-21 model parameters for the TBC layer [20]

Parameter	Value
A	0.93
B	0.31
C	0

M	0.6
N	0.6
HEL(GPa)	2.79
PHEL(GPa)	1.46
D1	0.005
D2	1
K_1 (GPa)	130.95
K_2 (GPa)	0
K_3 (GPa)	0

The water in the AWJ has the following properties: the density is 1000 kg/m^3, the cut-off pressure is 10^{-5} Pa, and the dynamic viscosity is 10^3 Pa.s [10]. The abrasive particles have the following properties: the density is 3420 kg/m^3, the shear modulus is 108 GPa, and the Poisson's ratio is 0.22 [21]. The parameters in the Gruneisen equation used for the water jet and abrasive particles are summarized in Table 2 [10, 21].

Table 2: The parameters in the Gruneisen equation for the water jet and abrasive particles [10, 21]

Materials	C(m/s)	S_1	S_2	S_3	γ
Water jet	1480	2.56	-1.986	0.2286	0.4934
Abrasive particles	9003	-3.06	2.350	-0.383	1

2.2.4 Boundary conditions and model design matrix

Three different AWJ processing parameters are considered, including incident angle, abrasive particle concentration, and impacting time. The design matrix for all the simulation cases is summarized in Table 3. The parameters are chosen using the same conditions as the previous

experimental study, as close as possible [8]. Other parameters, such as velocity, particle size, nozzle diameter, and target distance are kept constant. To match the experimental conditions, a static non-moving water jet was used. However, a moving water jet source can be modeled if needed.

In this paper, the simulation work was completed using the LS-DYNA software package by Livermore Software Technology Corporation. Additional coding was developed in the software to simulate the abrasive water jet. The total simulation time for each run is about 9 hours on a supercomputer, which has 256 compute nodes of IBM NeXtScale nx360 M4 servers. Each node is equipped with two Intel Xeon E5-2650 v2 8-core processors and 32 GB of RAM and 250 GB of local disk storage.

Table 3: Design matrix of processing parameters used in the model

Simulation case	Abrasive concentration (wt %)	Incident angle (°)	Impacting simulation time (ms)
A	1,3	30	20
B	1	30,45,60,90	20
C	1	30	7,14,21,28

2.3 Erosion analytical model

To quantify the coating removal efficiency, the erosion rate is investigated and compared with an analytical model. The removed mass from the TBC due to water jet impact needs to be quantified in order to evaluate the erosion rate. In the model, the eroded mass is characterized by the number of SPH particles whose particle density values are lower than the initial density. The mass for each SPH particle is a constant, and the density is defined as the mass per unit volume[22]. When the particles are scattered during impact, their densities are reduced.

An erosion model in brittle materials, based on the stress wave fracture mechanism was proposed by Zeng and Kim [23, 24] for the AWJ process. The total erosion volume (V_T) includes two components: one is caused by the plastic flow (V_p), and the other is due to the network cracking caused by impact induced stress waves (V_f) [23]:

$$V_T = V_p + V_f \tag{13}$$

The volume removal due to plastic flow, V_p, is calculated by:

$$V_p = \frac{mv^2}{4\sigma_f}\left(sin2\alpha - 4sin^2\alpha + 38.12vsin^3\alpha\sqrt{\frac{\rho_p}{\sigma_f}}\right) \tag{14}$$

And the volume removal due to network cracking V_f is determined by:

$$V_f = \frac{f_w\beta a\sigma_f mv^2 sin^2\alpha}{3\gamma E} \tag{15}$$

where γ is the fracture energy per unit area; m is the mass of a single particle; v is the particle velocity at impact; σ_f is the flow stress of target material; f_w is the proportional factor (W_c/W), E is the modulus of elasticity; a is the grain size of ceramics, α is the impact angle, and β = 14.33 - 6.25 sin 2.8v.

As the AWJ cutting is a multiple impact process, the total material removal cannot be calculated by the simple summation of the material removal of individual particle impacts. A constant efficiency coefficient C, which is determined from experiments, is incorporated to predict the averaged material removal of individual particles. Therefore, the theoretical erosion rate, R, is calculated to be [24]:

$$R = \frac{C\rho V\dot{m}}{m} = C\left[\frac{f_w\beta a\sigma_f\rho\dot{m}v^2 sin^2\alpha}{3\gamma E} + \frac{\rho\dot{m}v^2}{4\sigma_f}\left(sin2\alpha - 4sin^2\alpha + 38.12vsin^3\alpha\sqrt{\frac{\rho_p}{\sigma_f}}\right)\right] \tag{16}$$

3 Results and discussion

3.1 Effect of incident angle on the morphology of the impact pit

Figure 3a shows the simulated impact pit hole, at the incident angle of 90°. It is close to a circular shape. The predicted shape is in reasonably good agreement with the experiment result [8], as shown in Figure 3b.

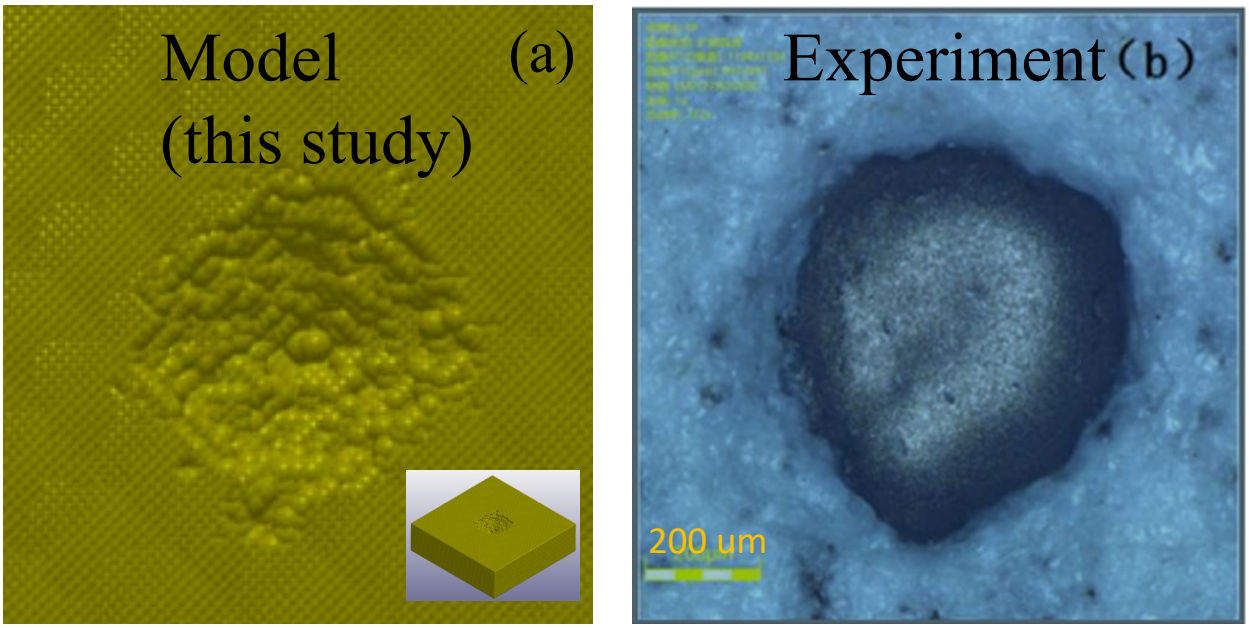

Figure 3: Impact pit hole (a) model prediction in this work. The inset in (a) is the simulated 3D view. (b) Experimental microstructure [8].

Figure 4a shows the cross-sectional views of the simulated impact pit holes with the incident angles of 30°, 45°, 60°, and 90°. The impact velocity is kept at 300 m/s and abrasive particle concentration is 1%. Overall, the depth of the impact pit holes increases with the incident angle, while the width of the impact holes decreases with the increase of the incident angle. Among different incident angles, the width of the incident angle 30° is the largest and the depth of the incident angle 90° is the largest. The simulated profiles, in terms of depth and width, are in the same trend as the

experimental measurements, as shown in Figure 4b. The incident angle effect is more distinguishable in the experiment because of its longer impact time.

Additionally, it is noted that all the profile curves, for both model and experiment, coincide at coordinates around (700 μm, 120 μm), and (1600 μm, 120 μm), suggesting there is a transition incident angle of 45°. When the AWJ incident angle is greater than the transition angle, impact holes develop faster in-depth direction than in the width direction.

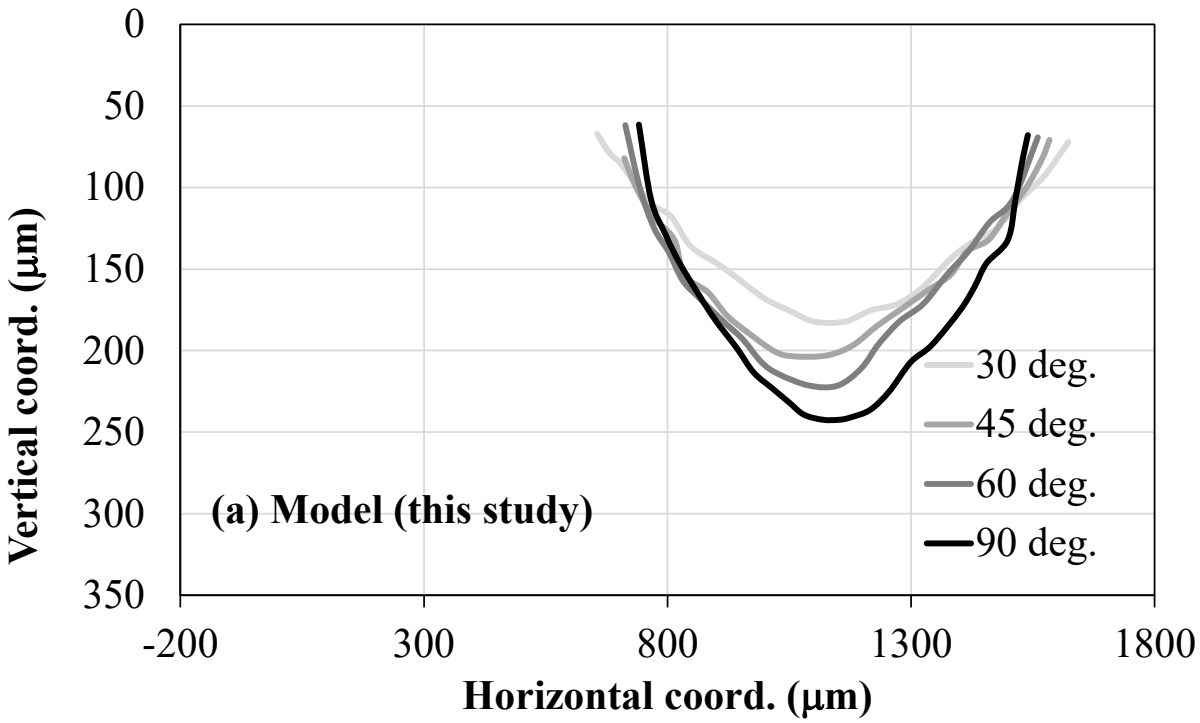

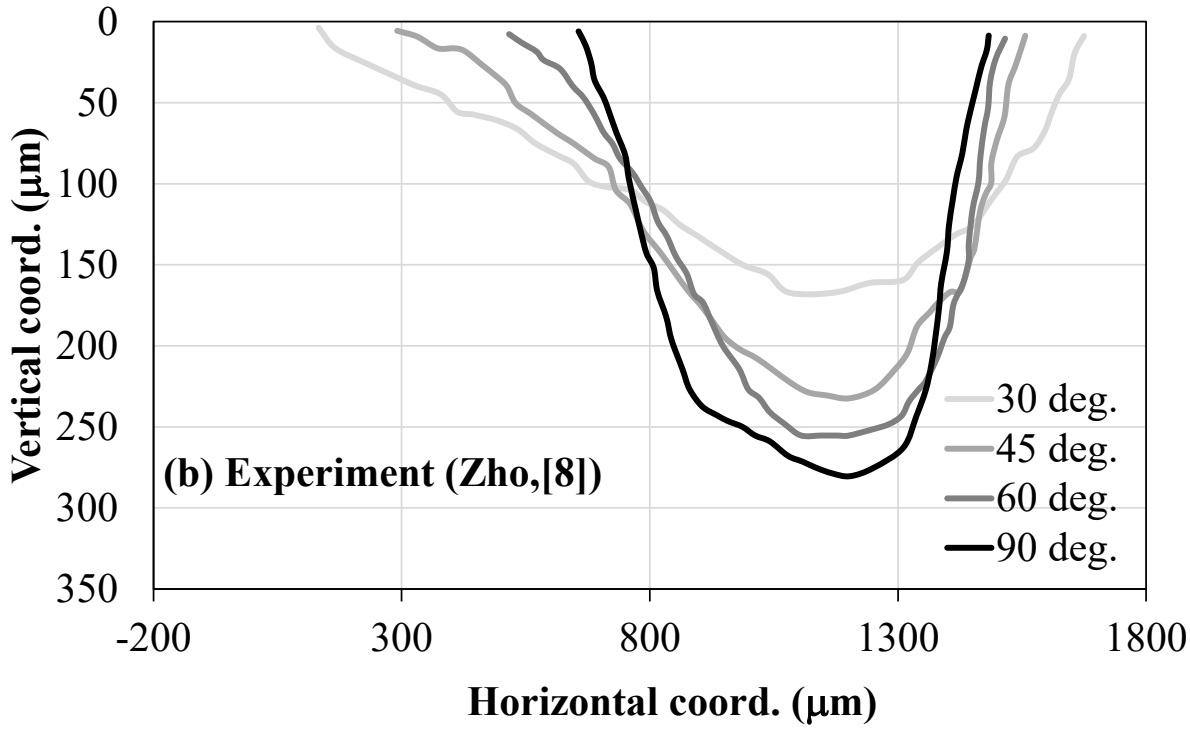

Figure 4: The cross-sectional profiles of the impact pit holes with different incident angles: 30°, 45°, 60°, and 90°. (a) Simulated results from this study, (b) experiment result from Ref. [8]. (Water jet direction is towards the left).

The incident angle's dependence on the hole profile can be attributed to the vertical velocity components. The vertical velocity component (Vz) of the AWJ process increases with the incident angle, following a sine function relation.

Figure 5 shows the relations between the depth and vertical velocity components. It shows that the depth increases with the vertical velocity component. This is because both the depth and vertical velocities share the same direction, and the kinetic energy from the AWJ process, $\frac{1}{2}mv^2$, is responsible for the erosion. The fitted curve using the 2nd order polynomial is shown in Figure 5, which confirms the validity of kinetic energy.

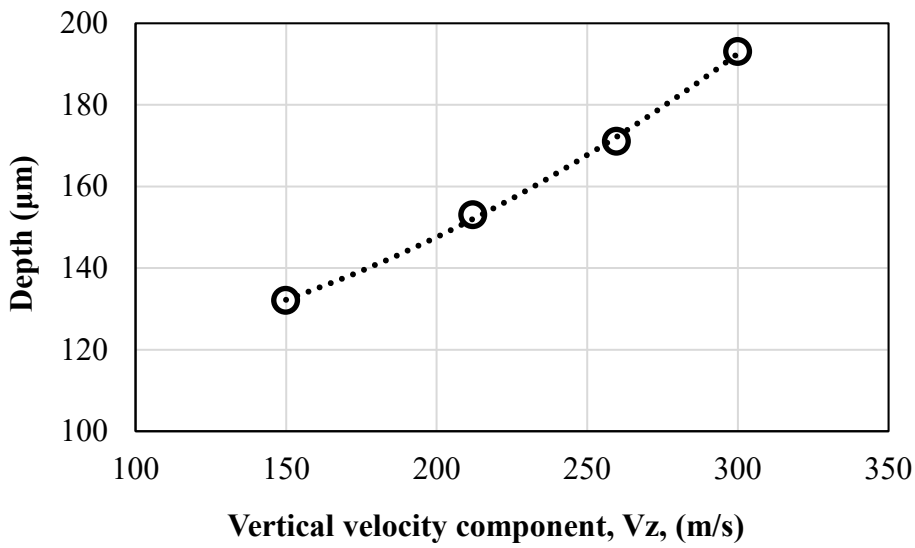

Figure 5: Pit hole depth's dependence on the vertical velocity component (Vz). The fitted curve using the 2nd order polynomial is also shown.

3.2 Effect of abrasive concentration on morphology of the impact pit

Figure 6 shows the cross-sectional views of the impact pit hole profiles with abrasive particle concentrations of both 1% and 3%. The impact velocity is 300 m/s and the incident angle is 30°. A higher concentration increases both the width and depth, which is consistent with the experimental data, as shown in Figure 6. However, our modeling results overpredict the 1% case and underpredict the 3% case. This may be due to the assumptions of perfect spherical shape and monosized particles used in our model.

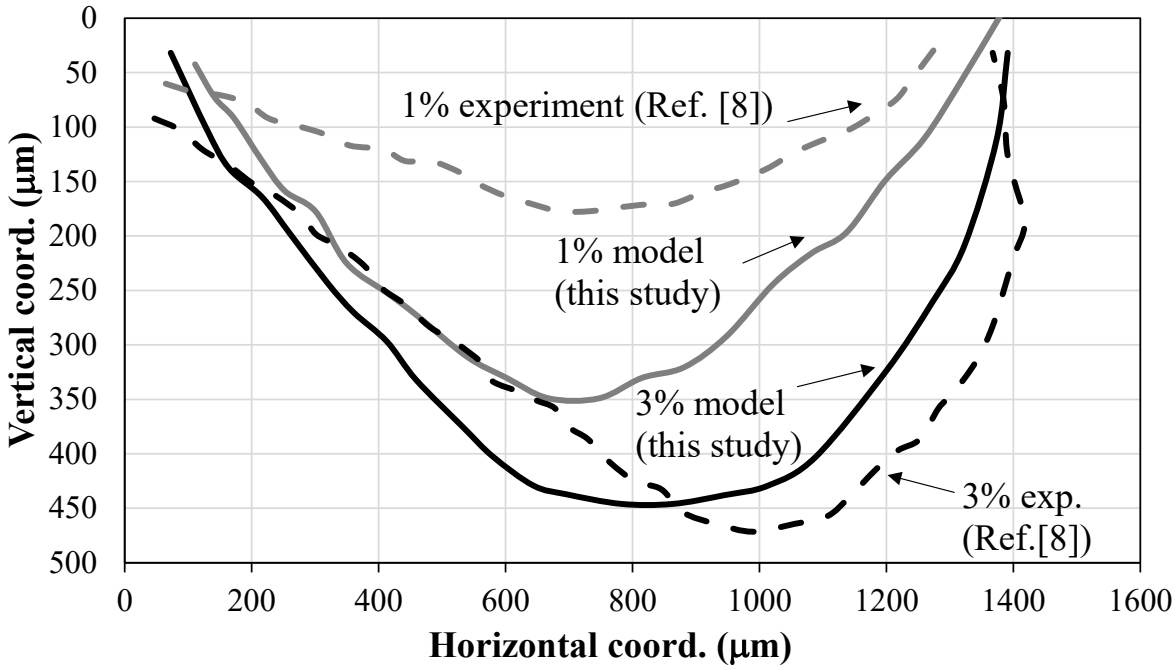

Figure 6: Cross-sectional views of impact pit hole profiles with abrasives (a) Simulated results, (b) experiment results [8]. (Water jet direction is towards the left).

3.3 Effects of impacting time on impact pit hole morphology

Figure 7 shows the cross-sectional views of the impact pit holes with the increasing impacting time, with a velocity of 300 m/s and an incident angle of 30°. Both the width and depth of the impact pit hole increase with impacting time. In this work, the time scaling factor between the model and experiment is 4.4×10^3, based on comparing the total simulation time and total experimental time. The scaling factor in the horizontal direction is determined to be 2.5.

It is noted that the deepest points in the pit hole shift gradually to the right, as labeled in Figure 7. This is because an incident angle of 30° is used. As the water jet is coming from the right side and towards the left side, the right side is eroded faster than the left side, causing the deepest points to

move to the right side. By comparing the eroded thickness, the right side is eroded about 1.5 times the left side. The phenomena are observed in both modeling and experimental results, which further illustrates the effectiveness of the SPH model.

It is also noted that the left side of the top surface in the experiment is much longer than the right side. This is unusual as it is unlikely to remove a quite large thin layer at the beginning of the process, i.e., 0.5 min. It is possible that there was a peel-off event of the top layer in the experiment which caused this abnormality.

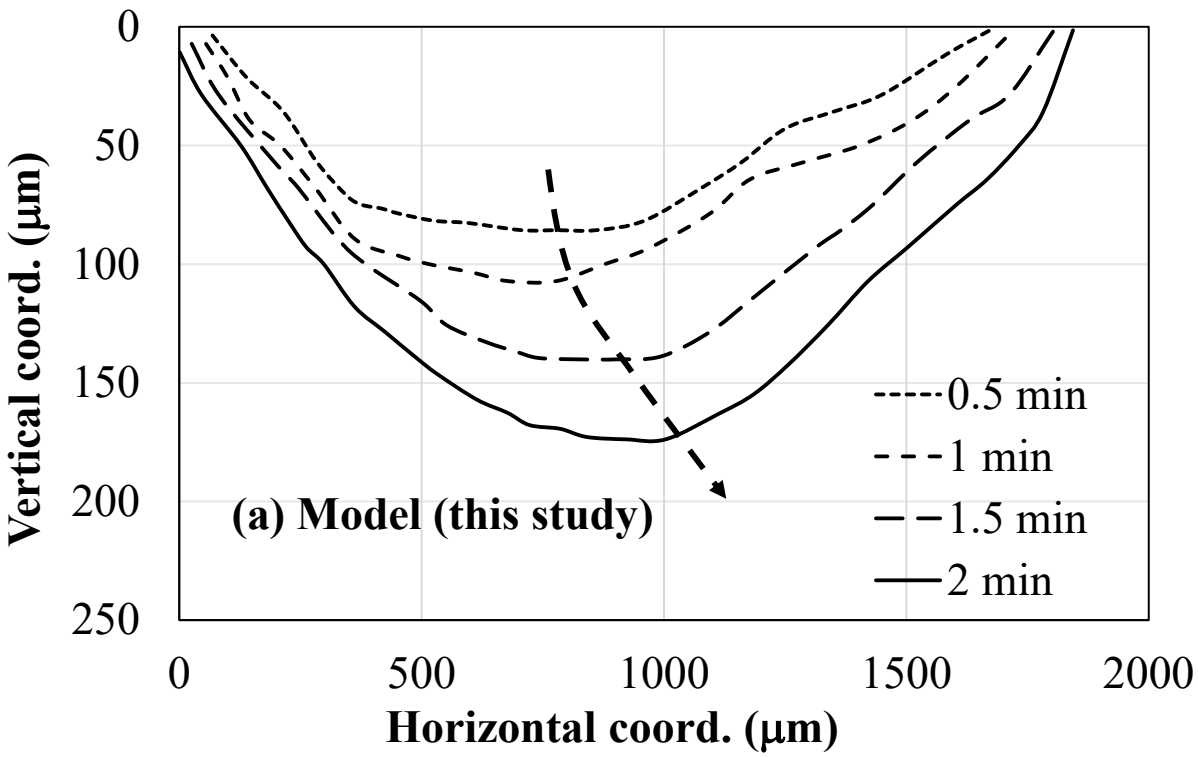

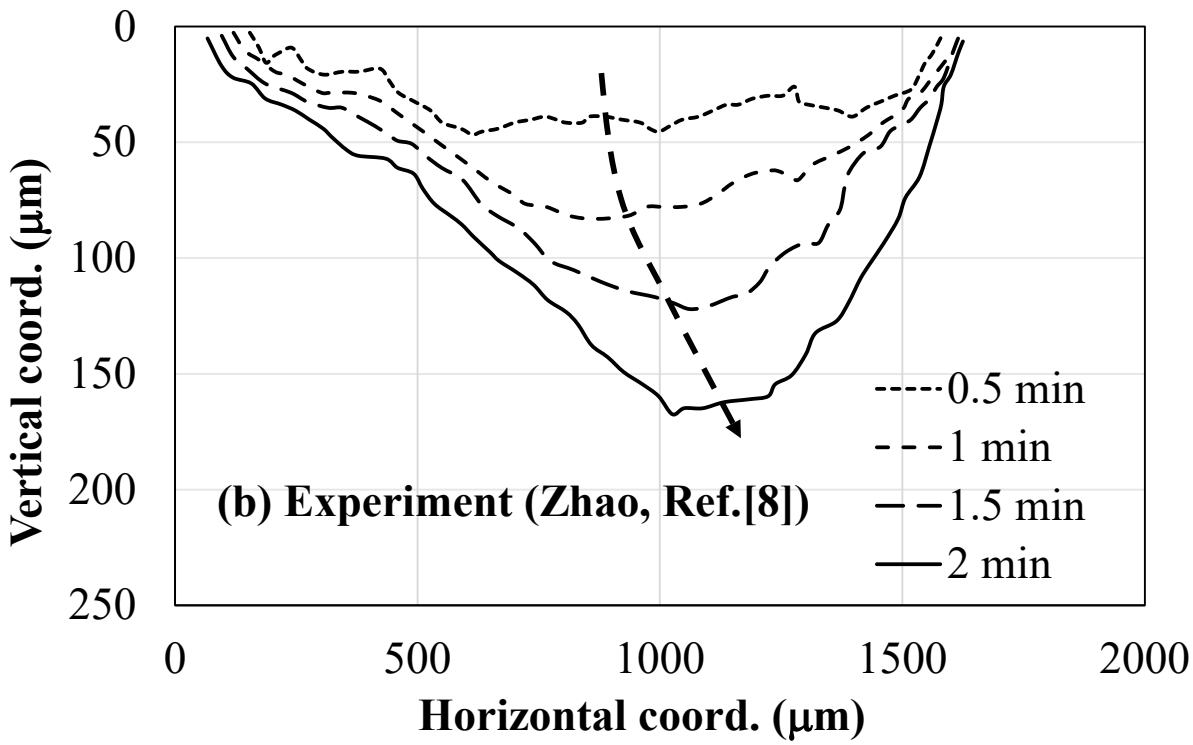

Figure 7: Cross-sectional views of the pit holes at different impacting times: (a) simulation results; (b) experiment results [8]. The curved arrows show the deepest points gradually shifting to the right as the AWJ process proceeds, due to 30o of incident angle.

3.4 Analytical erosion model

Based on the analytical erosion model presented in Equation 16 [24], the erosion rates at different incidence angles are calculated, as shown in Figure 8. The following parameters are used in the analytical model: f_w is 6.65×10^{-4}, γ is 5.8 J/m^2, σ_f is 23 GPa, a is 12 μm, and $\dot{m}$ is the particle flow rate, 12.9 g/s [23, 25, 26] . According to the SPH modeling results, the coefficient C is determined to be 0.0065.

As shown in Figure 8, the erosion rate increases with the incidence angle and the increase rate becomes slower as the incidence angle approaches 90°, which shows a good agreement with the analytical model. This is because the kinetic energy from the AWJ is responsible for the erosion

process. As the incident angle increases, more vertical velocity component contributes to the kinetic energy.

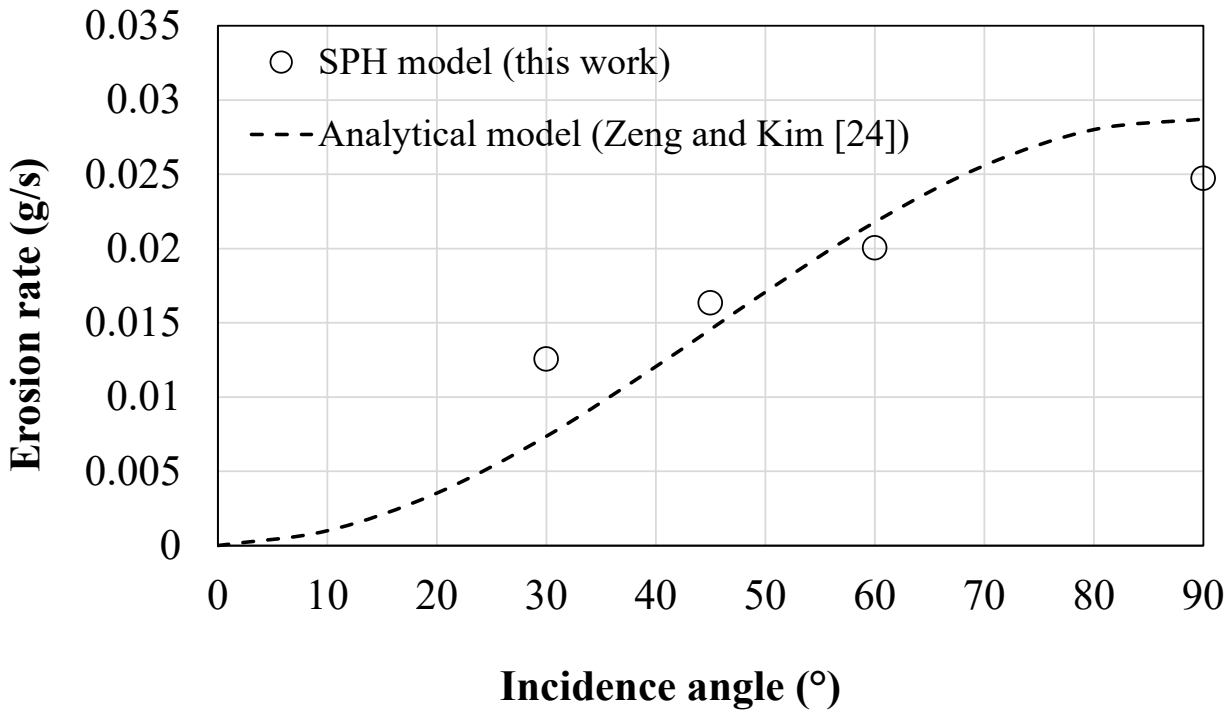

Figure 8: Simulated erosion rates at different water jet incident angles. The analytical model [24] is also included for comparison.

5 Conclusions

In this work, a new SPH based model to simulate the thermal barrier coating removal process using the abrasive water jet technique is developed. The effects of the water jet incident angle, abrasive particle concentration, and impacting time are investigated. The main conclusions are summarized as follows.

(1) Both the width and depth of the impact pit holes increase with impacting time. It is noted that the deepest points in the pit hole shift gradually to the right when a 30° water jet incident angle is used. This is because the water jet comes from the right side, which is more effective in removing the coatings on the right side. The phenomena are observed in both modeling and experimental results, which further illustrates the effectiveness of the SPH model.

(2) A higher concentration of water jet abrasive particles increases both the width and depth, which is consistent with the experimental data.

(3) The depths of the impact pit holes increase with the water jet incident angle, while the width of the impact holes decreases with the increase of the water jet's incident angle. The incident angle dependence can be attributed to the vertical velocity components.

(4) The erosion rate increases with the water jet incident angle, which shows a good agreement with the analytical model. As the water jet incident angle increases, more vertical velocity component contributes to the kinetic energy which is responsible for the erosion process.

Acknowledgment

This work is partially supported by the "Human Resources Program in Energy Technology (No. 20194030202450) and (No. 20181110100310)" of the Korea Institute of Energy Technology Evaluation and Planning (KETEP), and the National Research Foundation of Korea (NRF) grant funded by the Korea government (MSIP) (2018R1A5A6075959). The authors acknowledge the Indiana University Pervasive Technology Institute for providing supercomputer Karst's resources that have contributed to the research results reported within this paper.

References

1. Zhang, J. and Y.-G. Jung, *Advanced Ceramic and Metallic Coating and Thin Film Materials for Energy and Environmental Applications*. 2018: Springer International Publishing.
2. Murugan, M., et al. *Microstructure Based Material-Sand Particulate Interactions and Assessment of Coatings for High Temperature Turbine Blades*. in *ASME Turbo Expo 2017: Turbomachinery Technical Conference and Exposition*. 2017. American Society of Mechanical Engineers Digital Collection.
3. Yang, X., et al., *Removal and repair techniques for thermal barrier coatings: a review.* Transactions of the IMF, 2020. **98**(3): p. 121-128.
4. Bergs, T., et al., *Pure waterjet controlled depth machining for stripping ceramic thermal barrier coatings on turbine blades.* Procedia CIRP, 2019. **85**: p. 261-265.
5. Ahmed, T.M., et al., *Improving surface roughness of abrasive waterjet cutting process by using statistical modeling.* CIRP Journal of Manufacturing Science and Technology, 2018. **22**: p. 30-36.
6. Thompson, W., *Coating Removal for Turbine Components* in *Modern Machine Shop (https://www.mmsonline.com/articles/coating-removal-for-turbine-components, accessed 6/18/2021)*. 2011.
7. Kalpana, K., O. Mythreyi, and M. Kanthababu. *Review on condition monitoring of Abrasive Water Jet Machining system*. in *2015 International Conference on Robotics, Automation, Control and Embedded Systems (RACE)*. 2015. IEEE.
8. Zhao, K., et al. *Investigation of removing thermal barrier coatings from Nickel based super-alloy using abrasive water jet*. in *IOP Conference Series: Materials Science and Engineering*. 2018. IOP Publishing.
9. Liu, X., et al., *Effect of Abrasive Concentration on Impact Performance of Abrasive Water Jet Crushing Concrete.* Shock and Vibration, 2019. **2019**: p. 1-18.
10. Shahverdi, H., M. Zohoor, and S.M. Mousavi, *Numerical simulation of abrasive water jet cutting process using the SPH and ALE methods.* 2011.
11. Guo, L., S. Deng, and X. Yang, *Numerical simulation of abrasive water jet cutting chemical pipeline based on SPH coupled FEM.* Chemical Engineering Transactions, 2016. **51**: p. 73-78.
12. Ngangkham Peter Singh, D.S.S., *N. Ramesh Babu, *Thermal Analysis of Abrasive Waterjet Machining Process*, in *Proceedings of 10th International Conference on Precision, Meso and Nano Engineering*. 2017: India.
13. Liu, G.R., M.B. Liu, and S. Li, *"Smoothed particle hydrodynamics — a meshfree method".* Computational Mechanics, 2004. **33**(6): p. 491-491.
14. Liu, G.R. and M.B. Liu, *Smoothed Particle Hydrodynamics*. 2003: WORLD SCIENTIFIC. 472.
15. Liu, G.-R. and Y.-T. Gu, *An introduction to meshfree methods and their programming*. 2005: Springer Science & Business Media.
16. Guha, A., R.M. Barron, and R. Balachandar, *An experimental and numerical study of water jet cleaning process.* Journal of Materials Processing Technology, 2011. **211**(4): p. 610-618.
17. Cronin, D.S., et al. *Implementation and validation of the Johnson-Holmquist ceramic material model in LS-Dyna*. in *Proc. 4th Eur. LS-DYNA Users Conf*. 2003.

18. Zhao, Z., et al., *Dynamics simulation of photonic crystal fiber end face polishing.* Advances in Mechanical Engineering, 2017. **9**: p. 168781401771181.
19. Hallquist, J.O., *LS-DYNA keyword user's manual.* Livermore Software Technology Corporation, 2007. **970**: p. 299-800.
20. Denga, B., et al., *Smoothed particle hydrodynamics (SPH) simulation and experimental investigation on the diamond fly-cutting milling of zirconia ceramics.* Procedia CIRP, 2019. **82**: p. 202-207.
21. Vahedi, K. and N. Khazraiyan. *Numerical modeling of ballistic penetration of long rods into ceramic/metal armors*. in *8th International LS-DYNA Users Conference*. 2004.
22. Schulson, E.M., *Structure and mechanical behavior of ice.* JOM, 1999. **51**(2): p. 21-27.
23. Zeng, J. and T.J. Kim, *An erosion model for abrasive waterjet milling of polycrystalline ceramics.* Wear, 1996. **199**(2): p. 275-282.
24. Zeng, J. and T.J. Kim, *An erosion model of polycrystalline ceramics in abrasive waterjet cutting.* Wear, 1996. **193**(2): p. 207-217.
25. Kumar, A.N. and B.F. Sørensen, *Fracture energy and crack growth in surface treated Yttria stabilized Zirconia for SOFC applications.* Materials Science and Engineering: A, 2002. **333**(1-2): p. 380-389.
26. Tang, F. and J.M. Schoenung, *Evolution of Young's modulus of air plasma sprayed yttria-stabilized zirconia in thermally cycled thermal barrier coatings.* Scripta Materialia, 2006. **54**(9): p. 1587-1592.